Energy-Balance Control of PV Cascaded Multilevel Grid-Connected Inverters under Level-Shifted and Phase-Shifted PWM Modulations

Javier Chavarría, Domingo Biel, *Member IEEE*, Francesc Guinjoan, *Member IEEE,* Carlos Meza *Member IEEE* and Juan J. Negroni, *Member IEEE*

***Abstract*— This paper presents an energy-balance control strategy for a cascaded single-phase grid-connected H-bridge multilevel inverter linking *n* independent PV arrays to the grid. The control scheme is based on an energy-sampled data model of the PV system and enables the design of a voltage loop linear discrete controller for each array ensuring the stability of the system for the whole range of PV arrays operating conditions. The control design is adapted to Phase-Shifted and Level-Shifted Carrier PWM to share the control action among the cascade-connected bridges in order to concurrently synthesize a multilevel waveform and to keep each of the PV arrays at its maximum power operating point. Experimental results carried out on a 7-level inverter are included to validate the proposed approach.**

***Index Terms*— Cascaded-H bridge inverters, discrete-time control, grid-connected PV systems, multilevel modulations**

I. Introduction

A low-carbon society is a current political trend in developed countries which promotes, among others, the connection of photovoltaic (PV) systems to the electrical grid. These systems can contribute to clean electricity production as they are harmless for the environment and reduce the dependence on polluting fossil fuels such as coal, oil, gas and nuclear. Additionally, the power scalability of PV generation facilitates its large-scale penetration and leads to grid-connected applications ranging from few kilowatts of small-residential PV systems primarily installed on roofs to several megawatts of large-scale PV power plants.

Nevertheless, since the cost per watt of the PV system is still high compared to other energy sources, current research focuses in both reducing manufacturing costs and increasing the energy production of the overall system. In particular, the power conditioning stage interfacing the PV modules to the grid has caught the attention of researchers since it must account for maximum power extraction from the energy source and an optimal energy transfer to the grid [1]. In this concern, string and multi-string power conditioning architectures have been proposed over the last two decades to improve the features of the central inverter based one [2-6].

Among the power converter topologies adopted in the aforementioned architectures, multilevel inverter ones are being investigated as an interesting option for grid-connected PV systems [7-19]. In particular, the cascaded H bridge multilevel inverter (CHB-MLI) topology as depicted in Fig.1 is especially attractive for grid-connected PV applications for several reasons, for instance [2], [8], [10]:

a) The output voltage level required for grid power injection can be achieved without the use of a transformer as the voltage boosting is shared between the DC series connection of PV modules and the cascade connection of H bridge outputs.

b) This topology allows the connection of independent strings of PV modules to the input DC links of the power stage. Since the DC link voltages can be independently controlled, the maximum power extraction of a reduced number of PV modules can be accomplished with the help of maximum power point tracking (MPPT) algorithms. This improves both PV system reliability and energy production when the PV modules operate under mismatching conditions such as in the case of partial shadowing.

c) Like other multilevel inverter topologies, the CHB-MLI allows the synthesis of staircase AC output waveforms with lower total harmonic distortion (THD) compared to those generated by two-level based inverters, thus releasing output filter requirements for the compliance of grid harmonic standards. Depending on the operation power level, this synthesis can be carried out either at the fundamental

Manuscript received August 17, 2011. This work was supported in part by the Spanish Ministry of Science and Innovation and EU FEDER funds under the Grants DPI2009-14713-C03-03, DPI2010-15110 and RUE CSD2009-00046, Consolider-Ingenio 2010 Programme.

Javier Chavarría, Domingo Biel and Francesc Guinjoan are with the Electronic Engineering Department, Universitat Politècnica de Catalunya, 08034 Barcelona, Spain. (emails: javier.chavarria@upc.edu; domingo.biel@upc.edu ; francesc.guinjoan@upc.edu)

Carlos Meza, is with the Electronic Engineering Department, Instituto Tecnológico de Costa Rica, Cartago, Costa Rica. (email: cmeza@itcr.ac.cr)

Juan Negroni, is with the Electronic Engineering Department, Universidad Tecnológica Metropolitana, Santiago, Chile. (email: juan.negroni@utem.cl).

frequency [20] or at higher switching frequencies using multicarrier-based modulations [8], [10], [21], [22].

As shown in Fig.1, the control strategy of the CHB-MLI requires a set of voltage controllers to ensure independent voltage control of each PV array, a current controller driving the injected grid-current to assure overall power transfer at unity power factor and multilevel modulation to synthesize the staircase output voltage with low THD.

Except in the recent work of Cecati et al. [12] which suggests a fuzzy control approach to implement an extended version of this strategy allowing reactive power control, aforementioned controllers have been typically designed by continuous time linear control techniques. For instance, continuous time PI voltage controllers can be found in [15] and more recently in [16] which design follows the guidelines suggested in [23]. However, as pointed out in [24], these designs do not address system stability for the whole irradiance and temperature operating ranges since the nonlinear parametric dependence of the system resulting from the nonlinear current to voltage characteristics of the PV arrays is neglected.

Regarding output current control and multilevel modulation techniques, nonlinear current controllers based on sliding mode control and multiband hysteresis modulations operating at a variable switching frequency have recently been reported [18], [25]. However, linear PI or proportional resonant (PR) current controllers [26], [27] and fixed-frequency multicarrier-based PWM modulations are preferred in low power applications to facilitate the design of the reactive components. In this regard and to the author's knowledge, only PS-PWM (Phase Shifted PWM) has been applied to the CHB-MLI for grid-connected applications [15], [16], [19].

Collecting previous results [18-19], [24], the work here reported presents the design of a discrete-time linear voltage controllers for independent voltage control of each PV array, thus ensuring system stability for the whole irradiance operating range. Assuming a linear PR current controller, the paper also describes the design of the control signals driving each H-bridge for PS-PWM to further extend the results to LS-PWM (Level Shifted Carrier PWM).

The paper is organized as follows: the PV system modeling and the control strategy definition are presented in section II. Section III focuses on the energy-balance control approach and sets controller design criteria. Section IV addresses the generation of control signals driving the PV inverter switches for PS and LS-PWM modulations. Several different tests carried out on a 7-level inverter prototype linking three independent PV arrays to the grid are presented in section V for both modulations to experimentally verify the proposed approach. Finally, section VI draws the conclusions of this work.

II. System Modelling and Control Strategy Definition

The grid-connected PV multilevel inverter under study is shown in Fig.1. It comprises n PV generators and a power conditioning unit including n full-bridge inverters whose outputs are series-connected to the grid. Each PV generator is connected at the input of one full-bridge. This section introduces the formal mathematical modeling of the system and the control strategy to be designed.

A. PV generators

All PV generator are formed by an array of series-connected PV panels with identical PV cells. The current-to voltage relationship of the k^{th} PV generator can be extrapolated from the PV cell model of Prince et al. [28] as follows:

$$i_{PVk} = I_{gk} - I_{satk}\left(e^{\left(\frac{v_{Ck}}{\eta_k V_{Tk}}\right)} - 1\right) \quad k = 1,\ldots, n \tag{1}$$

where i_{PVk} and v_{Ck} are the output current and voltage respectively of the k^{th} PV generator, I_{gk} represents the light-induced current, η_k stands for the emission coefficient, I_{satk} is the reverse saturation current and V_{Tk} represents the thermal voltage of the semiconductor material. This model assumes that each generator can operate at different irradiance and temperature levels, i.e, each generator can exhibit a different Maximum Power Point (MPP) at any time.

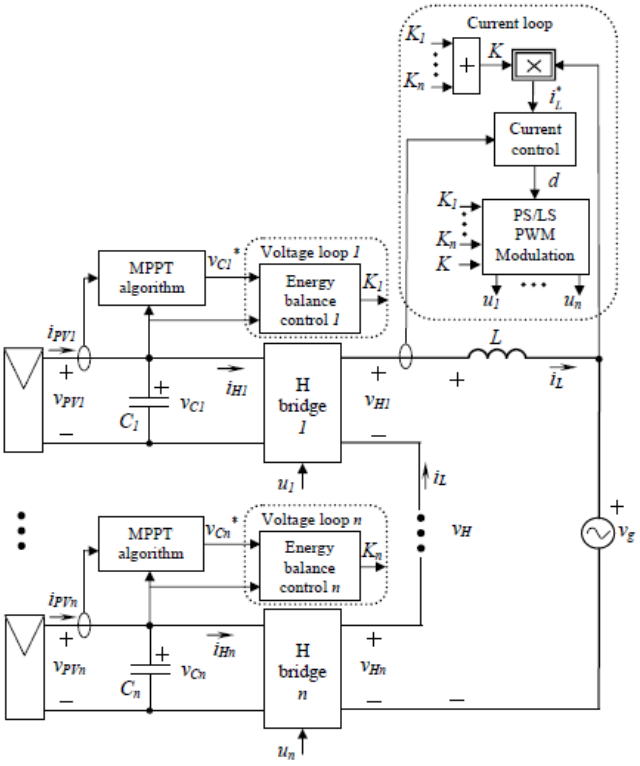

Fig.1. Grid-connected PV multilevel inverter.

B. Power conditioning unit

As for the variables in Fig.1, the k^{th} cascaded-bridge can be modeled as follows if no losses are considered:

$$\begin{cases} v_{Hk} = u_k v_{Ck}; & k = 1,2,\ldots,n \\ i_{Hk} = u_k i_L; & k = 1,2,\ldots,n \end{cases} \tag{2}$$

where u_k stands for the control signal of each full-bridge which is assumed to operate under three-level modulation, thus restricting the values of the control signal to $u_k \in \{-1,0,1\}$. The

lossless operation of each inverter cell can be derived in terms of instantaneous power since from (2) the following identity holds:

$$v_{Ck} i_{Hk} = v_{Hk} i_L \tag{3}$$

The output voltage of the cascaded inverters, v_H is given by:

$$v_H = \sum_{k=1}^{n} v_{Hk} = \sum_{k=1}^{n} u_k v_{Ck} \tag{4}$$

Finally, the system dynamics can be modeled by the following set of differential equations:

$$C_k \frac{dv_{Ck}}{dt} = i_{PVk} - u_k i_L; \quad k = 1,...n \tag{5a}$$

$$L \frac{di_L}{dt} = \sum_{k=1}^{n} u_k v_{Ck} - v_g(t) \tag{5b}$$

where v_g represents the grid voltage, which is assumed to be purely sinusoidal, i.e.

$$v_g(t) = A \sin(\omega_g t) \tag{6}$$

being ω_g the grid angular frequency. It is worth noting that the dynamic description of the PV system is given by (1), (5) and (6), and involves the nonlinear *i-v* relationship of the PV arrays.

C. Control strategy

The control of the multilevel inverter must achieve the following goals:

1. The operation of each PV generator at its own MPP independently of the ambient conditions, to assure the maximum power extraction of each array.
2. The transfer of the overall DC power to the grid. This is performed by the output current $i_L(t)$ which must be injected to the grid with low harmonic distortion at unity power factor.
3. The synthesis of a multilevel step-like AC wave voltage, $v_H(t)$, at the output of the cascaded converter.

The following paragraphs summarize the control strategy of the system according to the block-diagram in Fig.1.

The first goal requires the design of a voltage control loop per array which regulates the corresponding capacitor voltage v_{Ck} to a reference value given by a MPPT algorithm (v_{Ck}^* in Fig.1) at any time. This paper assumes that the above reference signals come from conventional Perturb & Observe MPPT algorithms [29].

With regard to the second goal, the injection of the DC power in phase with the grid entails the control of the output current i_L (i.e. the design of a current loop) to track with a fast transient and zero steady-state error a current reference i_L^* given by:

$$i_L^*(t) = K(t) v_g(t) = K(t) A \sin(\omega_g t) \tag{7}$$

where the current amplitude $K(t)A$ must be time varying to deal with the time varying input DC power. When the output current reaches this reference, the transfer condition of the overall average power over a grid period can be formulated as:

$$\frac{1}{T_g} \int_{(m-1)T_g}^{mT_g} \sum_{k=1}^{n} i_{PVk}(\tau) v_{Ck}(\tau) d\tau = \frac{1}{T_g} \int_{(m-1)T_g}^{mT_g} K(\tau) \left(A \sin(\omega_g \tau)\right)^2 d\tau \tag{8}$$

However since the temperature and irradiance vary slowly within a grid period, so varies the input DC power. Therefore the average DC power can be approximated as:

$$\frac{1}{T_g} \int_{(m-1)T_g}^{mT_g} \sum_{k=1}^{n} i_{PVk} v_{Ck} d\tau \approx \sum_{k=1}^{n} i_{PVk(m-1)} v_{Ck(m-1)}$$

This assumption allows the value of $K(t)$ to be updated only at the beginning of each grid period, i.e.:

$$K(t) = K_{(m-1)} \quad for \quad (m-1)T_g \le t \le mT_g \; ; m = 1,2,...$$

Accordingly, the current reference given in (5) can be rewritten as:

$$i_L^*(t) = K_{(m-1)} A \sin(\omega_g t) \tag{9}$$

hence the transfer condition of the average power given in (8) becomes:

$$\sum_{k=1}^{n} i_{PVk(m-1)} v_{Ck(m-1)} = K_{(m-1)} A^2/2 \tag{10}$$

In other words, if the current controller drives the output current to properly track a current reference given by (9-10), the overall average DC power is transferred to the grid. In particular, if this power is set to its maximum value by the voltage controllers, the maximum power transfer is achieved. It is worth noting that this approach leads to discrete-time relationships among the system variables sampled at the grid period, as proposed for the control design of high-power-factor preregulators [30-32].

Finally, the design of the "modulation" block of Fig.1 focus on the last control goal. The block contains the same number of PWM modulators and cascaded inverter cells and delivers the control signals u_k driving each bridge. These signals are built based on both the information of the current loop which is related to the overall power transfer (d in Fig.1) and the information of the voltage loops ($K_1,..., K_n$ in Fig.1) which, in turn, is related to the power handled by each inverter. The multilevel step-like AC output voltage v_H is synthesized using PWM techniques based on Phase-Shifted (PS) and Level-Shifted (LS) triangular carriers. The details of the generation of these control signals for both modulations are addressed in section IV.

A direct attempt of control design from the system dynamics given in (1), (5) and (6) is cumbersome due, among others, to the current to voltage nonlinear relationship of the PV generators described in (1). The following approach undertakes this design to ensure at least the local stability of the system.

III. ENERGY-BALANCE CONTROL APPROACH

A. Energy-balance linear modeling

In terms of instantaneous power, the system can be characterized by the following power-balance equation:

$$\sum_{k=1}^{n} i_{PVk} v_{Ck} = \sum_{k=1}^{n} v_{Ck} C_k \frac{dv_{Ck}}{dt} + L i_L \frac{di_L}{dt} + i_L v_g \tag{11}$$

Assuming that the output current i_L has reached the reference value i_L^* given in (9-10) and integrating over a grid period yields:

$$\int_{(m-1)T_g}^{mT_g} \sum_{k=1}^{n} i_{PVk} v_{Ck} d\tau = \sum_{k=1}^{n} \frac{C_k}{2} \left[v_{Ckm}^2 - v_{Ck(m-1)}^2 \right] + \frac{K_{(m-1)} A^2 T_g}{2} \tag{12}$$

If E_{PVkm} stands for the DC energy produced by the k^{th} PV array during the m grid period and E_{Ckm} is the energy stored in the capacitor, namely:

$$E_{PVkm} = \int_{(m-1)T_g}^{mT_g} i_{PVk} v_{Ck} d\tau \tag{13a}$$

$$E_{Ckm} = 0.5 C_k v_{Ckm}^2 \tag{13b}$$

(12) can be rewritten as the following dynamic energy-balance equation:

$$\sum_{k=1}^{n} \left[E_{Ckm} - E_{Ck(m-1)} \right] = \sum_{k=1}^{n} E_{PVkm} - \frac{K_{(m-1)} A^2 T_g}{2} \tag{14}$$

However, as pointed out in [24], the above dynamic description is still not complete since E_{PVkm} and E_{Ckm} are dependent one on another through the current to voltage nonlinear characteristic of the PV generator given in (1). From (1) and (13) this nonlinear dependence can be found as

$$E_{PVkm} = \int_{(m-1)T_g}^{mT_g} \sqrt{\frac{2}{C_k} E_{Ck}} \left[I_{gk} - I_{satk} \left(e^{\frac{\sqrt{(2/C_k) E_{Ck}}}{\eta_k V_{Tk}}} - 1 \right) \right] d\tau \tag{15}$$

This relationship can be linearized around a reference value E_{Ckm}^*, i.e.:

$$E_{PVkm} \approx E_{PVkm}^* + \delta_k (E_{Ckm} - E_{Ckm}^*) \tag{16}$$

where:

$$E_{PVkm}^* = E_{PVkm}(E_{Ckm}^*) \quad ; \quad \delta_k = \left. \frac{dE_{PVkm}}{dE_{Ckm}} \right|_{E_{Ckm} = E_{Ckm}^*} \tag{17a}$$

and, the slope δ_k can be expressed as:

$$\delta_k = \frac{T_g (I_{gk} + I_{satk})}{\sqrt{2 C_k E_{Ckm}^*}} - \frac{T_g I_{satk}}{\sqrt{2 C_k E_{Ckm}^*}} \exp\left(\sqrt{\frac{2 E_{Ckm}^*}{C_k \eta_k^2 V_{Tk}^2}} \right) \left(1 + \sqrt{\frac{2 E_{Ckm}^*}{C_k \eta_k^2 V_{Tk}^2}} \right) \tag{17b}$$

Replacing (16) into (14) leads to the following relationship which corresponds to a discrete-time linearized model of the grid-connected PV system:

$$\sum_{k=1}^{n} \left[E_{Ckm} - E_{Ck(m-1)} \right] = \sum_{k=1}^{n} \left[E_{PVkm}^* + \delta_k (E_{Ckm} - E_{Ckm}^*) \right] - \frac{K_{(m-1)} A^2 T_g}{2} \tag{18}$$

This model demonstrates that if the energy of each capacitor E_{Ckm} is regulated to the reference value E_{Ckm}^* corresponding to the k^{th} PV array, namely

$$E_{Ckm} = E_{Ck(m-1)} = E_{Ckm}^*; \quad k = 1, 2, ..., n \tag{19}$$

then, according to (13a), (18) collapses to (10), i.e.:

$$\sum_{k=1}^{n} E_{PVkm}^* = \sum_{k=1}^{n} i_{PVk(m-1)}^* v_{Ck(m-1)}^* T_g = \frac{K_{(m-1)} A^2 T_g}{2} \tag{20}$$

The desired power transfer is thus achieved. It must be pointed out that since the reference current and voltage values of each PV array are set by the irradiance and temperature operating conditions, the only way to force (20) is by controlling the variable $K_{(m-1)}$. To ensure energy control of all capacitors, a set of n auxiliary variables K_k with $k=1,...,n$ is defined so that:

$$\sum_{k=1}^{n} K_{k(m-1)} = K_{(m-1)} \tag{21}$$

and in this case (18) becomes:

$$\sum_{k=1}^{n} \left[E_{Ckm} - E_{Ck(m-1)} \right] = \sum_{k=1}^{n} E_{PVkm}^* + \sum_{k=1}^{n} \delta_k (E_{Ckm} - E_{Ckm}^*) - \sum_{k=1}^{n} \frac{K_{k(m-1)} A^2 T_g}{2} \tag{22}$$

Therefore if the dynamics of each bridge is modeled as:

$$E_{Ckm} - E_{Ck(m-1)} = E_{PVkm}^* + \delta_k (E_{Ckm} - E_{Ckm}^*) - \frac{K_{k(m-1)} A^2 T_g}{2}; \quad k = 1, ..., n \tag{23}$$

the auxiliary variable $K_{k(m-1)}$ can be controlled to set the capacitor energy to its reference value, this resulting in

$$\frac{K_{k(m-1)} A^2 T_g}{2} = E_{PVkm}^*; \quad k = 1, 2, ..., n \tag{24}$$

It is worth emphasizing that proper control of each auxiliary variable leads to the desired steady-state of the overall system given in (20) since from (21) and (23) it can be written:

$$\sum_{k=1}^{n} \frac{K_{k(m-1)} A^2 T_g}{2} = \frac{K_{(m-1)} A^2 T_g}{2} = \sum_{k=1}^{n} E_{PVkm}^* \tag{25}$$

Finally note that if the reference E_{Ckm}^* is set to the MPP of the PV arrays, the maximum power is transferred to the grid.

One of the main benefits of the previous approach is that a linear discrete-time model of the dynamics of each bridge is obtained. Applying the Z transform to (23) yields:

$$E_{Ck}(z) = \left[E_{PVk}^*(z) + \delta_k (E_{Ck}(z) - E_{Ck}^*(z)) \right] \frac{z}{z-1} - \frac{K_k(z) A^2 T_g}{2(z-1)}; \quad k = 1, 2, ..., n \tag{26}$$

This model allows the design of a linear discrete-time controller $G_{Ck}(z)$ to control the auxiliary variable $K_k(z)$ according to the block diagram derived from (26) and shown in Fig. 2:

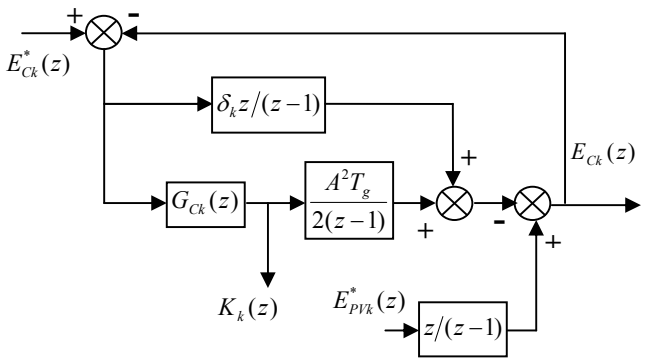

Fig.2. Block-diagram of the energy balance control for bridge *k*.

This controller is hereafter referred to as the "energy-balance controller" and is designed with the help of the powerful linear control tools in the Z domain to ensure the local stability of the corresponding control loop.

B. Control design guidelines for local stability

This section presents the main design guidelines for the controllers of the cascaded inverter. A complete design of a laboratory prototype built to experimentally verify the proposed approach is presented in section V.

B.1. Energy-balance controllers

The energy-balance controller design follows the same approach in [24], which is summarized below for the sake of completeness.

From the block-diagram of Fig. 2, the closed-loop transfer function can be written as

$$E_{Ck}(z) = \frac{zE^*_{PVk}(z) - E^*_{Ck}(z).\left[z\delta_k + 0.5A^2T_gG_{Ck}(z)\right]}{z - 1 - \left(z\delta_k + 0.5A^2T_gG_{Ck}(z)\right)}$$

A PI digital controller is chosen to ensure the control of E_{Ck} with zero steady-state error and to fix a desired transient response. Accordingly, $G_{Ck}(z)$ can be written as:

$$G_{Ck}(z) = \gamma_k \frac{z - \alpha_k}{z - 1}$$

Hence, the closed-loop characteristic equation, noted as $P_k(z)$, results in

$$P_k(z) = (1-\delta_k)z^2 + \left(\delta_k - 2 - \frac{\gamma_k A^2T_g}{2}\right)z + 1 + \frac{\gamma_k\alpha_k A^2T_g}{2} \quad (27)$$

The set of controller parameters γ_k and α_k ensuring the system stability is derived by applying the Jury test to (27), this yielding the following design restrictions:

$$\begin{cases} \delta_k < 1\,;\, \alpha_k < 1\,;\, \gamma_k < 0 \\ \dfrac{4(\delta_k - 2)}{A^2T_g(1+\alpha_k)} < \gamma_k < \dfrac{-2\delta_k}{\alpha_k A^2T_g} \end{cases} \quad (28)$$

Accordingly, the following design guidelines are adopted:

a) The zero of the controller (α_k) will be located close to the unit circle to compensate the destabilizing effect of the integral action.

b) The controller gain (γ_k) will be adjusted to ensure the stability conditions given in (28).

These restrictions involve the operating conditions of the PV arrays through the parameter δ_k defined in (17b).

C.2. Current controller

The energy-balance control approach assumes that the output current i_L has reached the reference i_L^*. This assumption requires the design of a current controller to ensure that i_L tracks the sinusoidal current reference i_L^* given in (9) with a fast transient response and zero steady-state error. The closed-loop dynamics of the inverter can be represented by the following block-diagram:

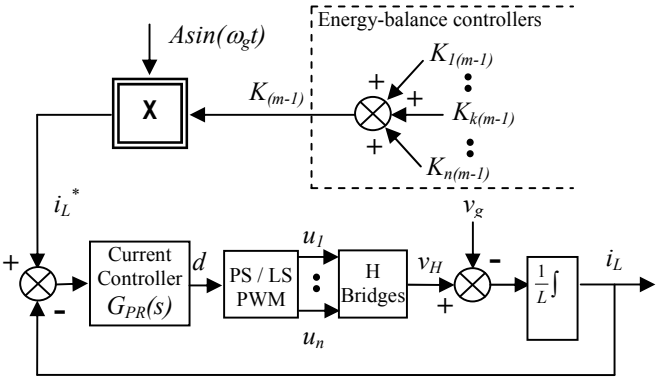

Fig.3. Block-diagram of the current control loop.

As extensively reported in [26-27], a linear Proportional + Resonant (PR) controller is especially suitable to track a sinusoidal current reference. The transfer function of this controller, $G_{PR}(s)$, is given by:

$$G_{PR}(s) = K_p + \frac{K_i s}{s^2 + \omega_g^2} \quad (29)$$

By following the design guidelines in [26-27], the controller concurrently ensures a fast dynamics, zero-steady state error at the tracking frequency and local stability.

IV. CONTROL SIGNALS FOR PS-PWM AND LS-PWM MODULATIONS

The proper operation of the current loop leads to a duty cycle *d* ensuring the transfer of the overall average DC power to the grid. The last step of the control design is the generation of the control signal of each modulator u_K from the duty cycle *d* to drive the power handled by each bridge according to the energy balance control. This generation depends on the modulation technique used to build the multilevel output voltage v_H. To show this dependence, Fig.4 illustrates the voltages of a 3 full-bridge cascaded inverter for the particular case of the same input normalized DC voltages when a sinusoidal signal of normalized amplitude is applied to PS-PWM (Fig.4a) and LS-PWM (Fig.4b) modulators operating at the same carrier frequency:

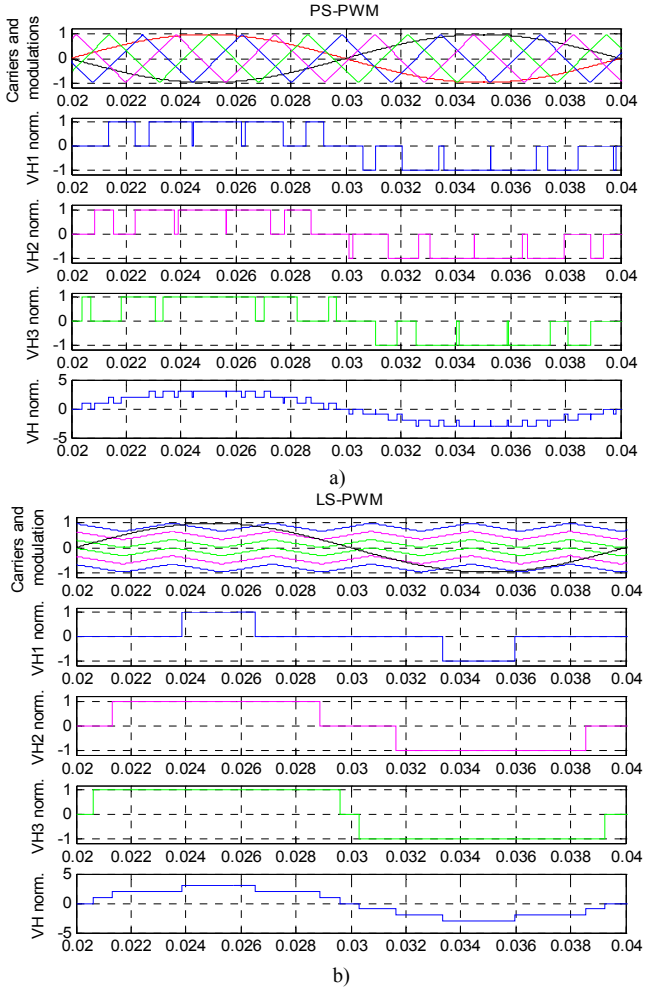

Fig. 4. Resulting voltages for a) PS-PWM and b) LS-PWM

As previously reported in [8], PS-PWM leads to an even power distribution among the inverters but to an uneven distribution if LS-PWM is applied,, as it can be seen from the output voltage plot of each bridge (v_{H1}, v_{H2}, v_{H3} of Fig.4a and b). However the work of Angulo et al. [33] modifies the LS-PWM strategy by introducing the concept of "rotating carrier" which allows the power balance by modifying the carrier assigned to each inverter over time. This concept periodically assigns to each inverter (with a period T_{rot}) the carriers of different shifted levels according to the sequence in Fig. 5, during the same time interval T_a. It is worth noting that achieving power balance requires both the sequence in Fig. 5 and the same time interval assignment.

In contrast, the case under study requires an unbalanced power distribution among the inverters to deal with different operating conditions of the PV arrays: the previous strategies must therefore be modified to make sure that each inverter handles the power of its corresponding PV array.

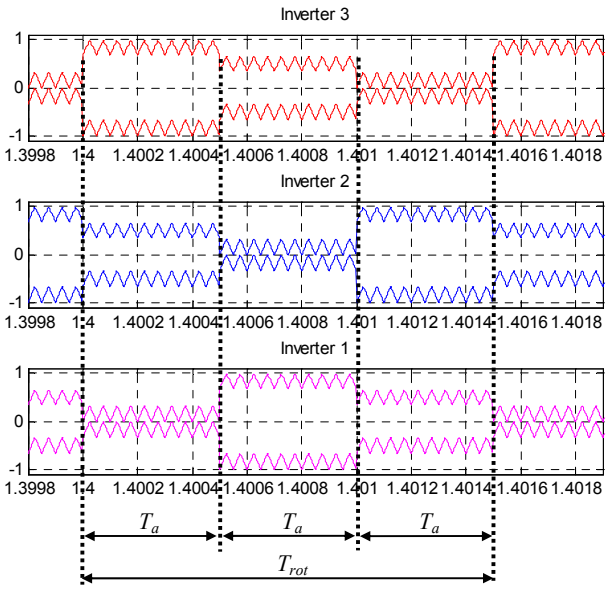

Fig. 5. Inverter rotating carrier assignment for LS-PWM

This modification is based on the fact that both the overall power handled by the cascaded-inverter and its distribution among the inverter cells can be known from the auxiliary control variables K_k applying (23) and (25). Accordingly, the PS and LS-PWM strategies are modified as follows:

A) PS-PWM:

The duty-cycle d_k of inverter k is computed as:

$$d_k = \frac{K_k}{\sum_{k=1}^{n} K_k} d = \frac{K_k}{K} d \tag{30}$$

The PS-PWM and the corresponding control signals are shown in Fig.6 for the case of 3 inverters:

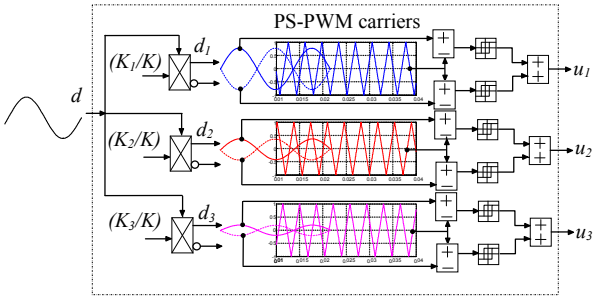

Fig.6. PS-PWM strategy

B) LS-PWM

For Level-Shifted modulation the control design takes advantage of the rotating carrier concept and applies the same rotating carrier assignment to each inverter as in Fig.5, but the time during which this assignment prevails is modified as:

$$T_k = \frac{K_k}{\sum_{k=1}^{n} K_k} T_{rot} = \frac{K_k}{K} T_{rot} \tag{31}$$

The resulting assignment is shown in Fig.7 for the case of

three inverters:

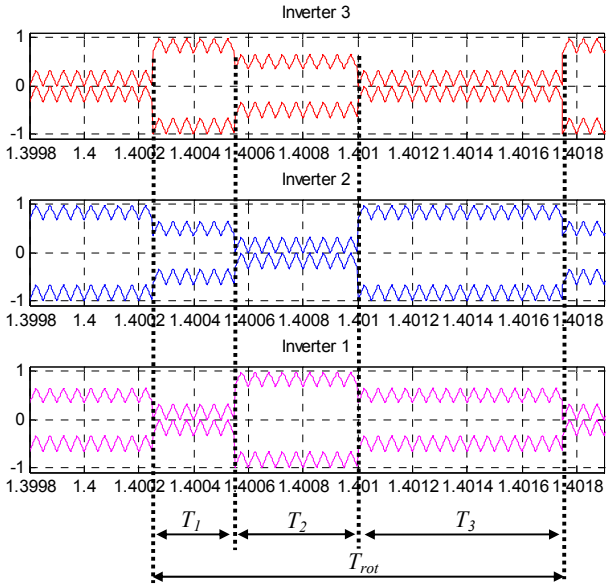

Fig.7. Modified LS-PWM modulation strategy

V. EXPERIMENTAL VALIDATION

A laboratory prototype of a grid-connected PV multilevel inverter including three cascaded inverter cells was built to experimentally verify the proposed approach. The energy-balance and current controllers described in Section III were implemented in a field programmable gate array (FPGA, Xilinx Spartan 3). The FPGA was used to generate the PS-PWM carriers and the rotating carriers of the LS-PWM addressed in section IV. It must be pointed out that the voltage references v_{Ck}^* (see Fig.1) were externally set since no MPPT algorithm was implemented because of its slow dynamics compared to that of the PV inverter. Nevertheless, an MPPT algorithm emulation was included in the tests. The experimental set-up is described in the following paragraphs:

A. Power stage and PV arrays

All the full-bridge switches were built by means of IRFP240 MOSFETs controlled by IR21084 drivers. The reactive components of the power stage were set to $C_1 = C_2 = C_3 = 2.2mF$ for the input capacitors and to $L=950\mu H$ for the output filter inductance. Three Solar Array Simulators (SAS) (Agilent E4350B #J02) were also used to emulate the electrical behavior of the PV arrays. The power vs voltage curves programmed in each SAS which correspond to three different solar incident irradiances are shown in Fig.8 and. The SAS were controlled through a GPIB bus using auxiliary software to allow the emulation of step irradiance changes.

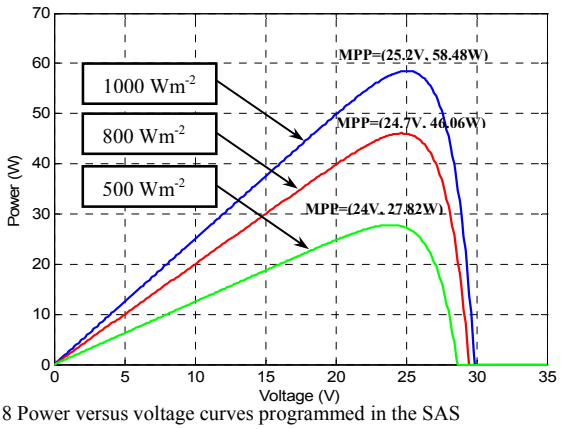

Fig. 8 Power versus voltage curves programmed in the SAS

Since the maximum SAS open circuit voltage is of 86V, the multilevel inverter prototype was connected to the single phase grid through a step-up power transformer of 20:3 turns ratio. This resulted in a grid voltage amplitude of $33V_{RMS}$ and a frequency of 50Hz at the transformer primary side. Therefore, the values of A and T_g were set to $A=33\sqrt{2}V$ and T_g=20ms.

B. Control Design

B1. Energy-balance controllers

The same energy-balance controller, referred to $G_c(z)$, was designed for the three arrays. The following design procedure assumes the worst operating case to ensure system stability over a wide range of operation.

As pointed out in section III.B.1, parameter α_k must be set to a value close to 1 to mitigate the instability effect of the integral component of G_c. Therefore, to focus on the selection of the parameter γ_k, α_k is fixed to 0.875.

The design of the controller gains (γ_k) is constrained by the stability conditions of (28) which depend on parameter δ_k. Moreover, the expression of δ_k given in (17b) must fulfill the stability restriction δ_k <1 for the whole range of irradiances under which the PV array operates. The worst case corresponds to the maximum irradiance value. Note from (17.b) that this restriction leads to the operating range of the array voltage (v_{Ck}) (i.e. of the capacitor stored energy E_{Ck}) ensuring the system stability under this irradiance. This range can be evaluated by a numerical simulation of δ_k vs v_{Ck} as shown in Fig. 9 for an irradiance of 1000W/m^2 and the parameters previously defined. As can be seen, the lower voltage limit of 22.35V is reached when δ_k=1 while the upper one of 30V corresponds to the open circuit voltage of the PV array.

In addition, (28) constrains the values of γ_k in terms of the parameter δ_k. Setting δ_k=0.9 to ensure the condition δ_k<1, the values of parameter γ_k ensuring system stability are constrained to: -0.053 <γ_k<-0.047. It can be proved that a value of γ_k=-0.05 assures system stability for a sufficiently wide operating range.

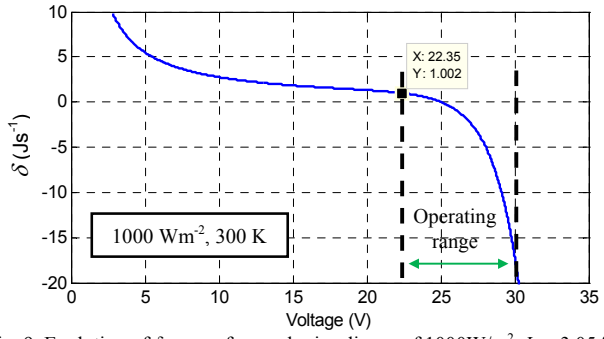

Fig. 9. Evolution of δ_k vs v_{Ck} for a solar irradiance of 1000W/m^2, I_g = 3.05A I_{sat}= 1.35·10^{-7}A, η = 1.

Fig. 10 shows the root locus of the system in terms of δ_k (see 27) for a fixed controller gain of γ_k=-0.05 and an irradiance of 1000W/m^2. The plot confirms the stability prediction and the system response is stable for δ_k <0.953 (or, equivalently, for a voltage v_{Ck}>22.59V). This stability condition requires that both capacitor voltage and voltage reference given by the MPPT algorithm remain within these limits at any time. Otherwise, the capacitor is pre-charged near the open circuit voltage of the PV array and regulated to an arbitrary voltage value falling within the stability limits. A partially or totally shaded panel will operate at the voltage arbitrarily fixed by the reference value if its natural operation falls out of the stability limits, as in the case of PV array voltage drop when by-pass diodes are turned-on.

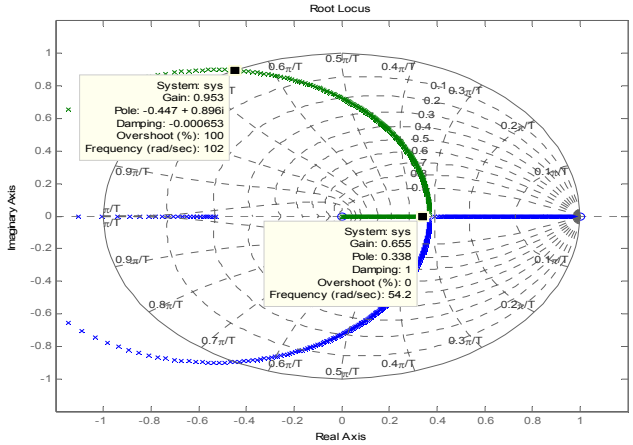

Fig. 10. Root locus for different values of δ_k when γ_k = -0.05. Variable δ_k is referred as "gain" in the root locus.

B.2 Current controller

Following the design procedure given in [26-27], the PR-controller parameters were fixed to K_p=140 and K_i=50000 to obtain a fast transient response and zero tracking error at the grid frequency.

B.3 Modulation parameters

The paper assumed the same value of the carrier frequencies in order to further make a coherent comparison in terms of harmonic distortion and overall efficiency for both modulations. The choice of the carrier frequency must take into account that the energy-balance control design is valid as long as the capacitor voltage remains within the validity range of the PV array linearized model. Note that, since the number of switching events per grid period is higher in PS-PWM (see Fig.4), the capacitor voltage dynamics is better controlled under this modulation. Accordingly, the carrier frequency must be designed for the LS-PWM case to ensure a number of switching events high enough to control the capacitor voltage within the validity range of the PV array linearized model. In this concern, the following criteria have been adopted:

1) A proper energy balance between the different inverter cells and the power delivered to the grid requires a minimum number of carrier rotations per grid period. The case under study has considered 9 rotations per grid period, being this number a multiple of the number of inverter cells. Hence, the rotating carrier period is T_{rot}=2,2ms, which has been finally adjusted to T_{rot}=2,15ms.

2) The number of carrier cycles during a rotation period must be high enough to preserve an acceptable resolution of the control action (i.e. the number of switching events) for any operating conditions of the PV arrays. In particular, as evidenced in Figs. 7 and 16, the resolution is compromised when, according to eq.(31), the lowest number of carrier cycles is assigned to the cell handling the lowest power. The case under study has adopted 42 carrier cycles per rotating period, to ensure an acceptable control action resolution for irradiances ranging from 500W/m^2 to 1000W/m^2. Moreover since this value is a multiple of the number of inverter cells, when all the PV arrays operate under the same irradiance, the same number of cycles, namely 42/3=14 cycles, are assigned to each inverter cell. On the other hand, each of the 6 carriers required in LS-PWM for the present design has been implemented into the FPGA by means of 512 levels, this finally leading to the following carrier frequency value:

$$f_{carrier} = \frac{1}{2 \cdot A_{carrier} \cdot div_{clk} \cdot T_{clk\,200MHz}} = \frac{1}{2 \cdot 512 \cdot 10 \cdot 5 \cdot 10^{-9}} = 19531Hz$$

where:

$A_{carrier}$ = Number of levels/carrier = 512;

div_{clk} = scaling factor of the FPGA clock signal = 10.

$T_{clk200MHz}$ = FPGA clock period = 5ns.

C. Experimental Results

A series of experimental tests were carried out to validate the proposed control approach. The design parameters of the experimental set-up are resumed in Table I:

TABLE I. DESIGN PARAMETERS OF THE PV INVERTER

Power stage	*MOSFET/drivers*	*IRFP240 /IR21084*
	C1 = C2 = C3	*2.2 mF*
	L	*950 μH*
Grid Voltage	*Transf. (20:3)*	*33V_{RMS} / 50 Hz*
Panels	*SAS Agilent*	*E4350B#J02*
Energy-balance controllers(FPGA)	γ_k	*-0.05*
	α_k	*0.875*
Current controller (FPGA)	K_p	*140*
	K_i	*50000*
Carrier frequency	f_c	*19.5 kHz*
Rotating period(LS-PWM)	T_{rot}	*2.15 ms*

Test 1—Start-up and steady-state behavior under uniform irradiance

The same power vs voltage curve corresponding to an irradiance of 1000W/m^2 (see Fig.8) was programmed in the three SAS and the reference voltages were set to v_{C1}^*= v_{C2}^*=v_{C3}^*=*25V*. Fig. 11 shows the start-up behavior of the inductor current (i_L) and the capacitor voltages (v_{C1}, v_{C2} and v_{C3}) for PS-PWM (left) and LS-PWM (right). As can be seen, the voltages evolve from the PV array open circuit voltages (30V) to the reference ones, and the transient response of the injected current is smooth. Fig. 12 presents the primary transformer voltage and the injected current (i_L) in steady state. Note that the output current is always in phase with the grid voltage. Fig. 13 shows the output voltage of the multilevel converter (v_H) and confirms that both modulations operate with seven levels, as expected. Fig. 13 also illustrates the injected current (i_L) and evidences a greater current amplitude ripple for LS-PWM. This is due to the different switching patterns of PS and LS modulations as confirmed by the spectrum of the injected current in Fig. 14: note how the first harmonic is located either at the carrier frequency (19.5kHz) for LS-PWM or at three times the carrier frequency (58.5kHz) for PS-PWM.

Moreover, Total Harmonic Distortion (THD), efficiency and displacement factor (i.e. phase shift φ between grid current and voltage) can also be extracted from these experimental results and are reported in Table II for both modulations:

TABLE II: QUALITY INDICES FOR PS AND LS PWM

INDEX	PS-PWM	LS-PWM
THD (%)	1,79%	1,95%
Efficiency (η%)	≈ 86%	≈ 86,8%
Cos(φ)	≈ 1	≈ 1

These results suggest that, under the same carrier frequency operation, both modulations exhibit an excellent displacement factor, thus confirming the proper operation of the P+R current controller. In addition, LS-PWM leads to better efficiency but worse THD than PS-PWM, this being attributable to the different switching patterns of both modulations. On the other hand, a FPGA-based design operating at a lower switching frequency to reduce switching losses would be envisaged for the PS-PWM case, but would result more difficult if LS-PWM is adopted since the lowest switching frequency is limited by both the ratio rotating frequency/grid frequency and the control action resolution supported by the FPGA platform, as detailed in section V B.3.

Test 2—Steady-state behavior under non-uniform irradiance

In this test the SAS were programmed to emulate system operation under three different irradiances, namely 1000W/m^2, 800W/m^2, and 500W/m^2 and the reference voltages were set to their MPP values, i.e. v_{C1}^*= *25.2V*, v_{C2}^*= *24.7V* v_{C3}^*=*24V* (see Fig. 8). Fig.15 shows a zoom of the steady-state capacitor voltages and confirms that they have reached their reference values. Since each inverter handles a different power, the control values delivered by the energy-balance controllers (K_k) were different, this leading to different duty cycles in PS-PWM (see 30) or different time interval assignation in LS-PWM (see 31). Fig. 16 shows a scaled version of the control signals internally generated by the FPGA for both modulations. As it can be seen in Fig.16 (left), inverters handling higher input power are driven by control signals of higher amplitude, in accordance with (30). Similarly, in (Fig.16 right), higher time intervals are assigned to inverters handling higher power, in accordance with (31).

Test 3 —Robustness to irradiance changes:

As can be deduced from Fig.2, the input E_{PVk}^* (i.e the energy of the PV array *k*) can be considered as a perturbation of E_{Ck} (i.e. the voltage of capacitor C_k). To check the robustness of the energy-balance control, the SAS were programmed to emulate an abrupt irradiance change according to the pattern in Table III and the reference voltage values were held at v_{C1}^*= v_{C2}^*=v_{C3}^*=*25V*. Fig. 17 shows the evolution of the capacitor voltages (v_{C1}, v_{C2} and v_{C3}) and the injected current (i_L). Note that, after a small transient response the voltage across the capacitors maintains its reference value, thus confirming a proper voltage regulation in the presence of irradiance changes.

TABLE III

Irradiance (W/m^2)	*Time interval (s)*			
	0 ≤t<1.6	*1.6 ≤t<5.2*	*5.2 ≤t<7.2*	*7.2 ≤t<10*
Irrad$_1$	*1000*	*800*	*800*	*800*
Irrad$_2$	*1000*	*1000*	*800*	*800*
Irrad$_3$	*1000*	*1000*	*1000*	*800*

Test 4—MPPT emulation:

The following two tests aimed to emulate an MPPT algorithm by varying the reference capacitor voltages. In the first test, all reference voltages were fixed at the same value which changed according to the pattern in Table IV. In the second one, the reference voltages simultaneously varied to different reference values following the pattern in Table V.

TABLE IV

	Reference Voltage (V)		
	0s ≤t<1.8s	*1.8s ≤t<6.4s*	*6.4s ≤t<10s*
v_{C1}^*	*25*	*28*	*25*
v_{C2}^*	*25*	*28*	*25*
v_{C3}^*	*25*	*28*	*25*

TABLE V

	Reference Voltage (V)	
	0s ≤t<3s	*3s ≤t<10s*
v_{C1}^*	*25*	*28*
v_{C2}^*	*25*	*25*
v_{C3}^*	*25*	*23*

Figs. 18 and 19 show the output current and the capacitor voltages for both tests and both modulations. As it can be seen, the capacitor voltages follow their respective voltage references after a short transient, validating the proposed control approach.

VI. CONCLUSIONS

This paper addresses the control design of a CHB-MLI grid-connected PV system which can operate under PS or LS Pulse Width Modulations. The energy-balance model of the system and the linearization of the PV array electrical characteristics allow the design of discrete-time PI linear voltage controllers ensuring independent control of PV arrays operation. This design which can be easily carried out by conventional discrete-time linear control techniques, takes into account the stability restrictions given by the Jury test which depend on the operating points of the PV arrays. In contrast to other works, the obtained criteria to choose the parameters of the controllers is one of the features of the proposed approach, since they ensure system stability for the whole operating range of the PV arrays in terms of irradiance and temperature. Furthermore, the definition of a set of auxiliary control variables allows the synthesis of the control signals driving each bridge not only for Phase Shifted PWM but also for Level Shifted PWM by modifying the rotating carrier concept.

A set of laboratory tests carried out on a 7-level CHB-MLI grid-connected PV system has experimentally validated the proper operation of the energy-balance control for both modulations under uniform and non uniform irradiance as well as under abrupt irradiance and MPPT algorithm changes. Moreover these results have also shown that LS-PWM leads to worse THD but better efficiency than PS-PWM. In this regard, a FPGA-based design operating at a lower switching frequency to reduce switching losses would be envisaged for the PS-PWM case, but would result more difficult if LS-PWM is adopted since the lowest switching frequency is limited by both the ratio rotating frequency/grid frequency and the control action resolution supported by the FPGA platform.

REFERENCES

[1] G. Petrone, G. Spagnuolo, R. Teodorescu, M. Veerachary, and M. Vitelli, "Reliability issues in photovoltaic power processing systems," *IEEE Trans. on Industrial Electronics*, vol. 55, no.7 pp. 2569–2580, July 2008.

[2] M. Calais, J. Myrzik, T. Spooner, V. G. Agelidis, "Inverter for Single-Phase Grid Connected Photovoltaic Systems – An Overview", PESC, Vol. 4, pp. 1995-2000, Feb. 2002.

[3] S. B. Kjaer, J. K. Pedersen, and F. Blaabjerg, "A review of single-phase grid-connected inverters for photovoltaic modules," *IEEE Trans. Ind. Appl.*., vol. 41, no. 5, pp. 1292–1306, Sep./Oct. 2005.

[4] M. Meinhardt and G. Cramer, "Multi-string converter: The next step in evolution of string-converter technology," in *Proc. 9th Eur. Conf. Power Electron. Appl*., 2001.

[5] G. Walker and P. Sernia, "Cascaded DC/DC converter connection of photovoltaic modules," *IEEE Trans. Power Electron*., vol. 19, no. 4, pp. 1130–1139, Jul. 2004.

[6] J.-M. Kwon, B.-H. Kwon, K.-H. Nam, "Grid-Connected Photovoltaic Multistring PCS With PV Current Variation Reduction Control," *IEEE Trans. on Industrial Electronics*, vol. 56, no. 11, pp. 4381-4388, Nov 2009.

[7] S. Daher, J. Schmid, and F. Antunes, "Multilevel inverter topologies for stand-alone PV systems," *IEEE Trans. on Industrial Electronics*., vol. 55, no. 7, pp. 2703–2712, Jul. 2008.

[8] M. Malinowski, K. Gopakumar, K.; J. Rodriguez, M.A. Pérez. "A Survey on Cascaded Multilevel Inverters" *IEEE Trans. on Industrial Electronics* vol 57, pp. 2197 – 2206, July 2010.

[9] M. Calais, V. G. Agelidis, and M. Meinhardt, "Multilevel Converter for Single-phase Grid-connected Photovoltaic Systems: An Overview," *Solar Energy*, Vol. 66, No. 5, pp. 325-335, 1999.

[10] J. Rodríguez, J. S. Lai and F.Z. Peng. "Multilevel Inverters: A Survey of Topologies, Controls and Applications". *IEEE Trans. on Industrial Electronics* vol 49 No. 4, pp. 724 – 738, August 2002.

[11] L. G. Franquelo, J. Rodriguez, J. I. Leon, S. Kouko, R. Portillo, and M. A. M. Prats, "The age of multilevel converters arrives," *IEEE Ind.Electron. Mag*., vol. 2, no. 2, pp. 28–39, Jun. 2008.

[12] C. Cecati,, F. Ciancetta., P. Siano. "A Multilevel Inverter for Photovoltaic Systems With Fuzzy Logic Control". *IEEE Trans. on Industrial Electronics* vol 57 No. 12, pp. 4115 – 4125, December 2010.

[13] S. Busquets-Monge, J. Rocabert, P. Rodriguez, S. Alepuz, J. Bordonau, "Multilevel Diode-Clamped Converter for Photovoltaic Generators With Independent Voltage Control of Each Solar Array," *IEEE Trans. on Industrial Electronics*, vol. 55, no. 7, pp. 2713-2723, July 2008.

[14] G. Grandi, C. Rossi, D. Ostojic, D. Casadei, "A New Multilevel Conversion Structure for Grid-Connected PV Applications," *IEEE Trans. on Industrial Electronics*, vol. 56, no. 11, pp. 4416-4426, Nov 2009.

[15] O. Alonso, P. Sanchis, E. Gubía, L. Marroyo, "Cascade H-Bridge Multilevel Converter for Grid Connected Photovoltaic Generators with Independent Maximum Power Point Tracking of each Solar Array," *2003 IEEE Power Electronics Specialists Conference*, pp.731-735.

[16] E. Villanueva, P. Correa, , J. Rodríguez, and M. Pacas, "Control of a Single-Phase Cascaded H-Bridge Multilevel Inverter for Grid-Connected Photovoltaic Systems. *IEEE Trans. on Industrial Electronics* vol 56 No. 11, pp. 4399 – 4406, November 2009.

[17] J. Selvaraj and N. A. Rahim, "Multilevel Inverter For Grid-Connected PV System Employing Digital PI Controller". *IEEE Trans. on Industrial Electronics* vol 56 No. 1, pp. 149 – 158, January 2009.

[18] J. J.Negroni, D. Biel, F. Guinjoan, C. Meza. "Energy-balance and sliding mode control strategies of a cascade H-bridge multilevel converter for grid-connected PV systems". *2010 IEEE Int.Conf. On Industrial Technology* pp.1155 – 1160.

[19] J.J. Negroni,F. Guinjoan, C. Meza, D. Biel, P. Sanchis. "Energy-Sampled Data Modeling of a Cascade H-Bridge Multilevel Converter for Grid-connected PV Systems". *10th IEEE International Power Electronics Congress*, pp. 1 – 6, 2006.

[20] Y. Liu, H. Hong, A. Q. Huang, "Real-Time Algorithm for Minimizing THD in Multilevel Inverters With Unequal or Varying Voltage Steps Under Staircase Modulation," *IEEE Trans. on Industrial Electronics*, vol. 56, no. 6, pp. 2249-2258, June 2009.

[21] B.P. McGrath, D. G. Holmes. " Multicarrier PWM Strategies for Multilevel Inverters". *IEEE Trans. on Industrial Electronics* vol 49 No. 4, pp. 858 – 867, August 2002.

[22] W.H. Lau, B. Zhou, H. Chung."Compact Analytical Solutions for Determining the Spectral Characteristics of Multicarrier-Based Multilevel PWM". *IEEE Trans. on Circuits and Systems-I,* vol 51 nº8, pp.1577-1585, August 2004.

[23] A. Dell'Aquila, M. Liserre, V. Monopoli, and P. Rotondo. "Overview of pi-based solutions for the control of DC buses of a single-phase H-bridge multilevel active rectifier," *IEEE Trans. Ind. Appl*., vol. 44, no. 3, pp. 857– 866, May/Jun. 2008.

[24] C. Meza , J.J. Negroni, D. Biel, F. Guinjoan. "Energy-Balance Modeling and Discrete Control for Single-Phase Grid-Connected PV Central Inverters". *IEEE Trans. on Industrial Electronics* vol 55 No. 7, pp. 2734 – 2743, June 2008.

[25] R. Gupta, A. Ghosh, and A. Joshi "Multiband Hysteresis Modulation and Switching Characterization for Sliding-Mode-Controlled Cascaded Multilevel Inverter". *IEEE Trans. on Industrial Electronics*,, Vol. 57, NO. 7, pp 2344-2353, July 2010.

[26] R. Teodorescu, F. Blaabjerg, M. Liserre and P.C. Loh. "Proportional-resonant controllers and filters for grid-connected voltage source converters". *IEE Proc.-Electr. Appl*., Vol. 153, No. 5, pp 750-762, September 2006.

[27] D. N. Zmood and D. G. Holmes. "Stationary Frame Current Regulation of PWM Inverters With Zero Steady-State Error". *IEEE Trans. on Power Electronics*, Vol. 18, No. 3, pp. 814-822, May 2003.

[28] M. Prince. "Silicon Solar Energy Converters". *J. Appl. Phys*., vol 26, no.5, pp. 534-540, May 1955.

[29] G. Petrone, G. Spagnuolo, M. Vitelli. "A Multivariable Perturb-and-Observe Maximum Power Point Tracking Technique Applied to a Single-Stage Photovoltaic Inverter". *IEEE Trans. on Industrial Electronics,* vol. 58, no. 1, pp. 76-84, January 2011.

[30] J. Kassakian, M. Schlecht and G.Verghese, *Principles of Power Electronics*. Norwell, MA: Addison-Wesley, 1991,pp. 395-399.
[31] K. Mahabir, G.Verghese, V.J. Thottuvelli, and A. Heyman, "Linear averaged and sampled data models for large signal control of high power factor ac-dc converters", *in Power Electron. Special. Conf. Rec*.,1990, pp.291-299.
[32] A. Mitwalli, S. Leeb, G. Verghese and V. Thottuvelil, "An adaptive digital controller for a unity power factor converter," *IEEE Trans.Power Electron.*, vol. 11, pp. 347-382, Mar. 1996.
[33] M. Angulo, P. Lezana, S. Kouro, J. Rodriguez, J., Bin Wu "Level-shifted PWM for Cascaded Multilevel Inverters with Even Power Distribution". *2007 IEEE Power Electronics Specialists Conference,* pp. 2373 – 2378.

Javier Chavarria was born in Tortosa, Spain, in 1978. He received the Technical Telecommunications Engineering degree in 2001, the M.S. and the Master in Electronics Engineering degrees in 2010 from the Universitat Politècnica de Catalunya (UPC), Barcelona, Spain. He was a Researcher in the Department of Electronic Engineering, Escola Politècnica Superior d'Enginyeria de Vilanova i la Geltrú, Spain. From 2001 to 2002, he was with CITCEA, UPC,, Barcelona, Spain. From 2002 to 2011 he was working as a Hardware Engineer with SONY design department, Barcelona, Spain. Since 2011, he is working as R&D Senior Electrical Engineer with Idneo Technologies S.L., Barcelona, Spain. Mr. Chavarria is collegiate member of the Spanish Official College of Technical Telecommunications Engineers (COITT), from which he won two prizes on 2001 and 2002, respectively. He is currently developing his Ph.D. research on power electronics studies at the UPC.

Domingo Biel (S'97-M'99) received the B.S, M.S. and Ph.D. degrees in telecommunications engineering from the Technical University of Catalonia, Barcelona, Spain, in 1990, 1994 and 1999, respectively. Since 2001, he is Associate Professor at the Electronic Engineering Department, Technical University of Catalonia (Spain), where he teaches power electronics and control theory.

He is the coauthor of 10 papers in international journals and more than 50 communications in international conferences. His research fields are related to nonlinear control and its application to renewable energy systems and power electronics.

Francesc Guinjoan (M'92) received the Ingeniero de Telecomunicación and Doctor Ingeniero de Telecomunicación degrees from the Universitat Politecnica de Catalunya (UPC), Barcelona, Spain, in 1984 and 1990, respectively, and the Docteur es Sciences degree from the Université Paul Sabatier, Toulouse, France, in 1992. He is currently Associate Professor with the Departamento de Ingenieria Electrónica, Escuela Técnica Superior de Ingenieros de Telecomunicación Barcelona, (UPC), where he teaches courses on power electronics. He has co-authored more than 80 papers in international journals and conferences and in 2011 he has been guest co-editor of the Special Issue on "Smart Devices for Renewable Energy Systems" of Transactions on Industrial Electronics. His research interests include power electronics modelling and control for renewable energy systems.

Carlos Meza (S'00 - M'07) received the B.S. degree in Electronic Engineering from the Costa Rica Institute of Technology, Cartago, Costa Rica, the M.Eng. degree in Embedded Systems Design from the ALaRI Institute, University of Lugano, Lugano, Switzerland, and the Ph.D. degree in Advanced Automation and Robotics from the Technical University of Catalonia, Barcelona, Spain, in 2001, 2003 and 2007 respectively. He has been a visiting researcher at the University of Groningen, Groningen, The Netherlands. From 2007 to 2009 he worked at the Institute of Applied Sustainability for the Built Environment, SUPSI, Cannobio, Switzerland. Currently he is a professor and researcher at the Electronic Engineering Department of the Costa Rica Institute of Technology, Cartago, Costa Rica, where he is the coordinator of the Laboratory of Electronic Systems for the Sustainability (SESLab). His main research interests are nonlinear dynamics, nonlinear control and renewable energy systems

Juan J. Negroni (M'04) received the degree in Electronics Engineering from the Universidad Tecnológica Metropolitana del Estado de Chile, Santiago, Chile, and the Ph.D. degree in Electronics Engineering from the Universitat Politecnica de Catalunya, Barcelona, Spain, in 2007. Since 1999, he has been an Associate Professor with the Department of Electric Engineering, Universidad Tecnológica Metropolitana del Estado de Chile, where he teaches courses on power electronics, He is the project leader of "Chilectra-UTEM" dealing with PV grid-connected systems and he also participates in research and innovation for the EU-LA group and for the R&D group "Proteinlab-UTEM". His research interests include power electronics for renewable energy systems.

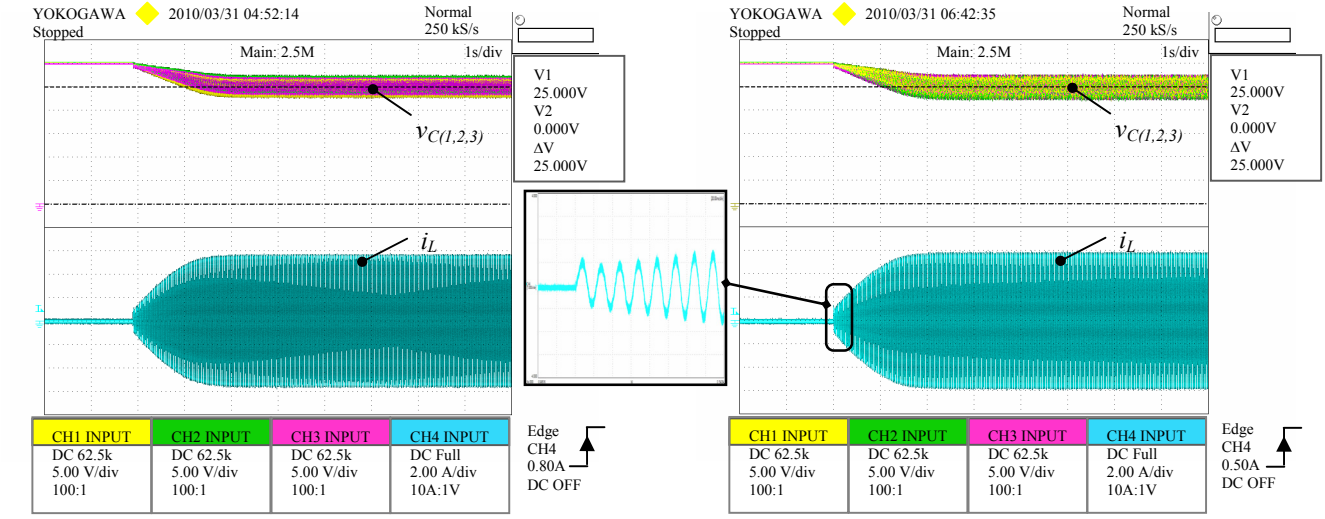

Figure 11. Start up behavior of inductor current (i_L) and capacitor voltages (v_{C1}, v_{C2} and v_{C3}) for both PS-PWM (left) and LS-PWM (right).

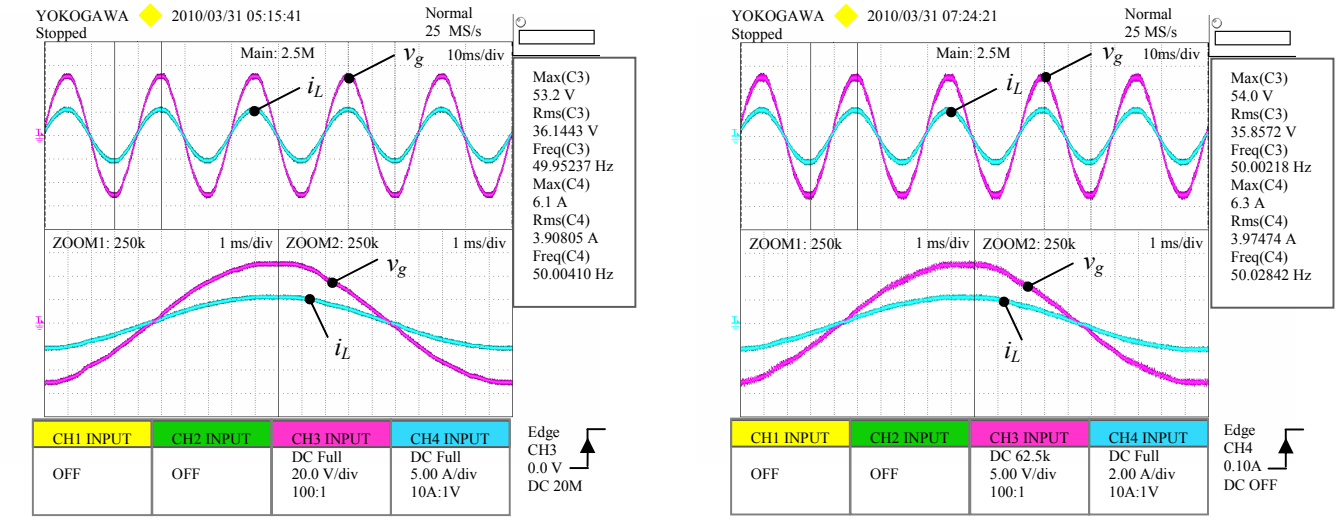

Figure 12. Steady state primary transformer voltage and injected current (i_L) for both PS-PWM (left) and LS-PWM (right).

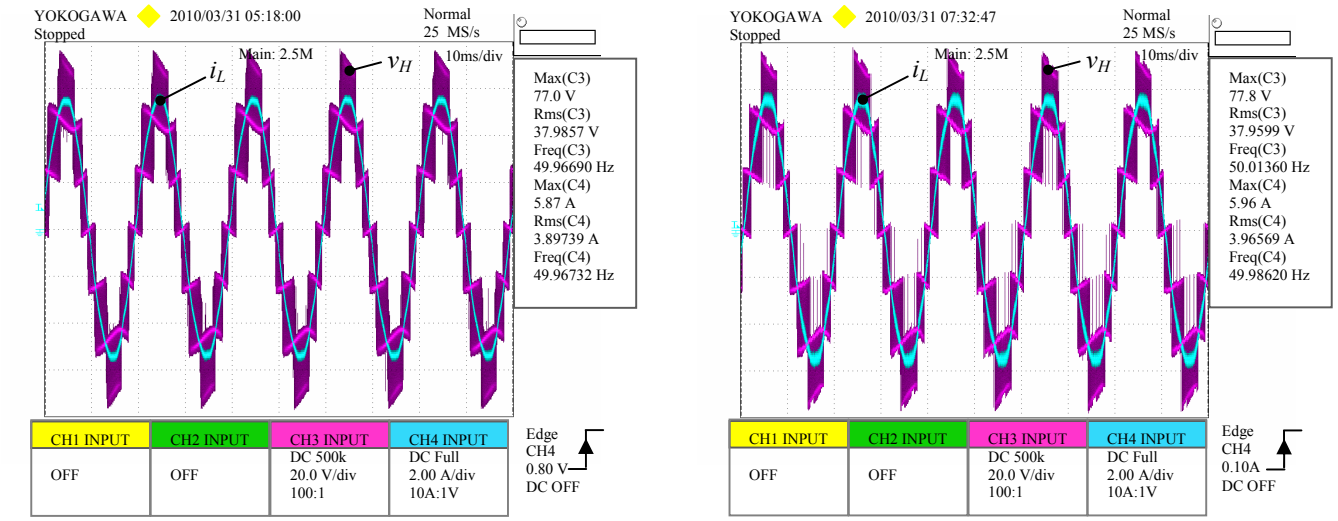

Figure 13. Steady state output voltage of the multilevel converter (v_H) and injected current (i_L) for both PS-PWM (left) and LS-PWM (right).

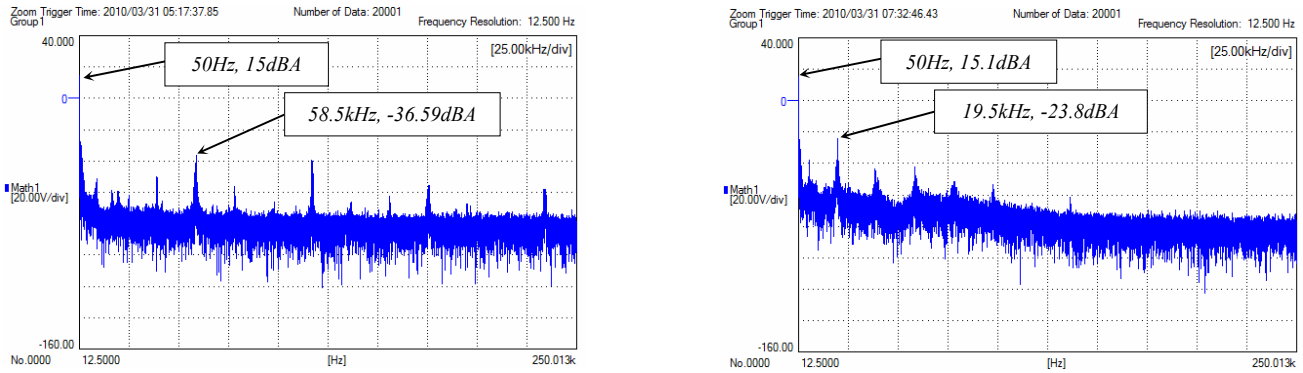

Figure 14. Spectrum of the inductor current of the multilevel converter: PS-PWM (left) and LS-PWM (right).

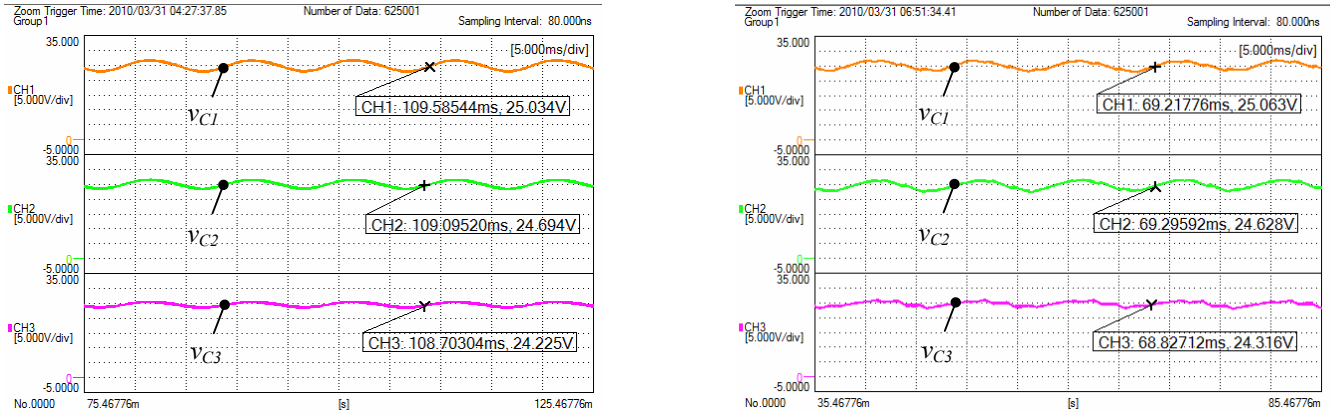

Figure 15. Zoom of the capacitor voltages: PS-PWM (left); LS-PWM (right)

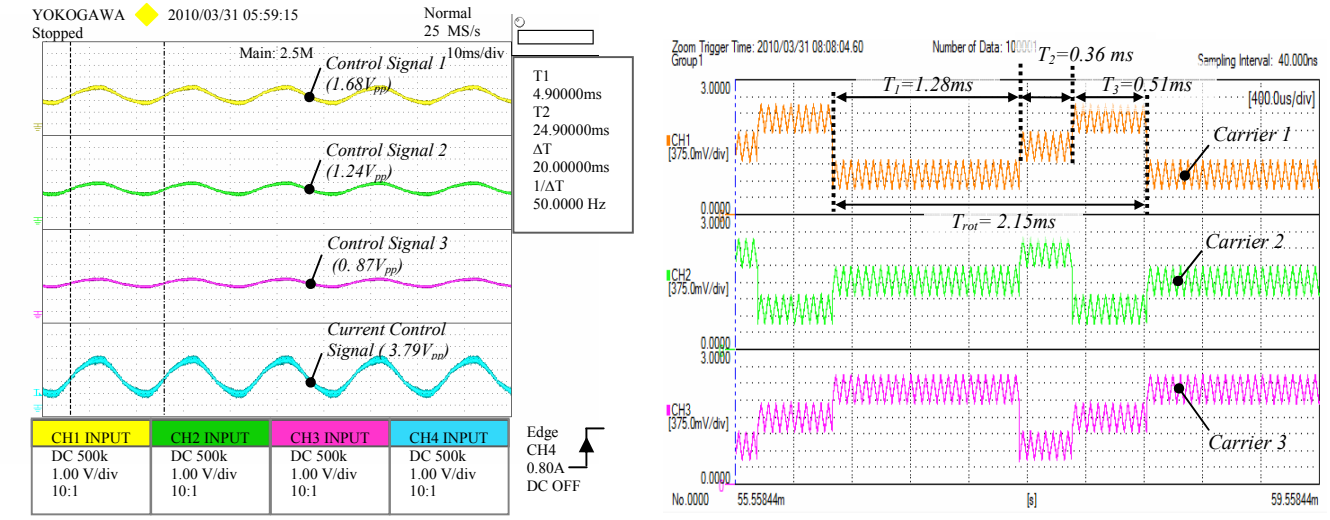

Figure 16. Steady state PS-PWM control signals (left). Zoom of steady state LS-PWM sequence assignation (right).

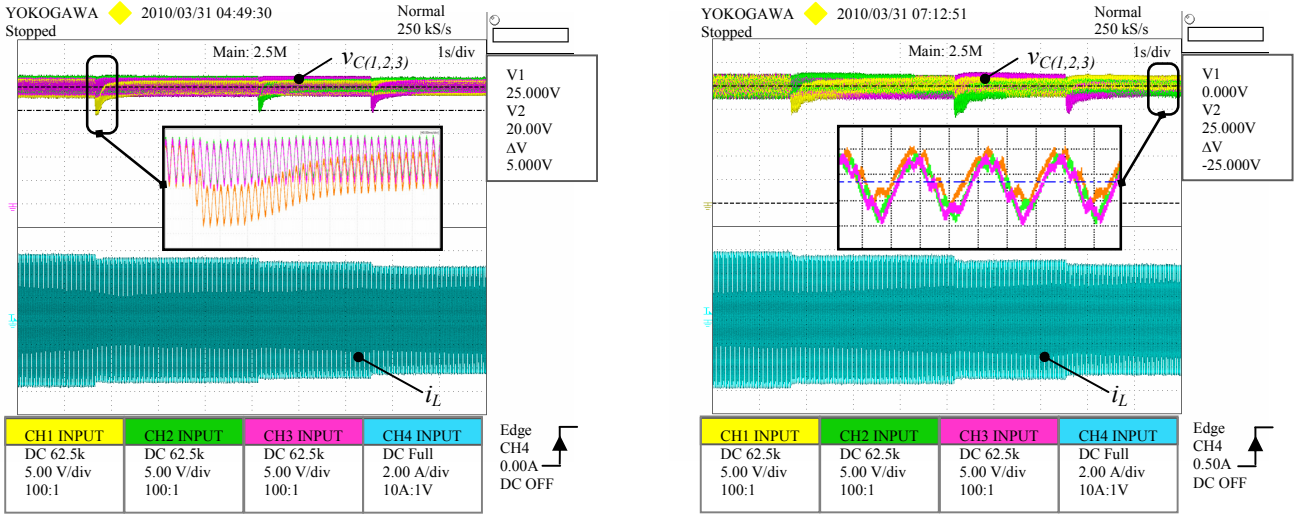

Figure 17. Irradiance change. Inductor current (i_L) and capacitor voltages (v_{C1}, v_{C2} and v_{C3}) for both PS-PWM (left) and LS-PWM (right).

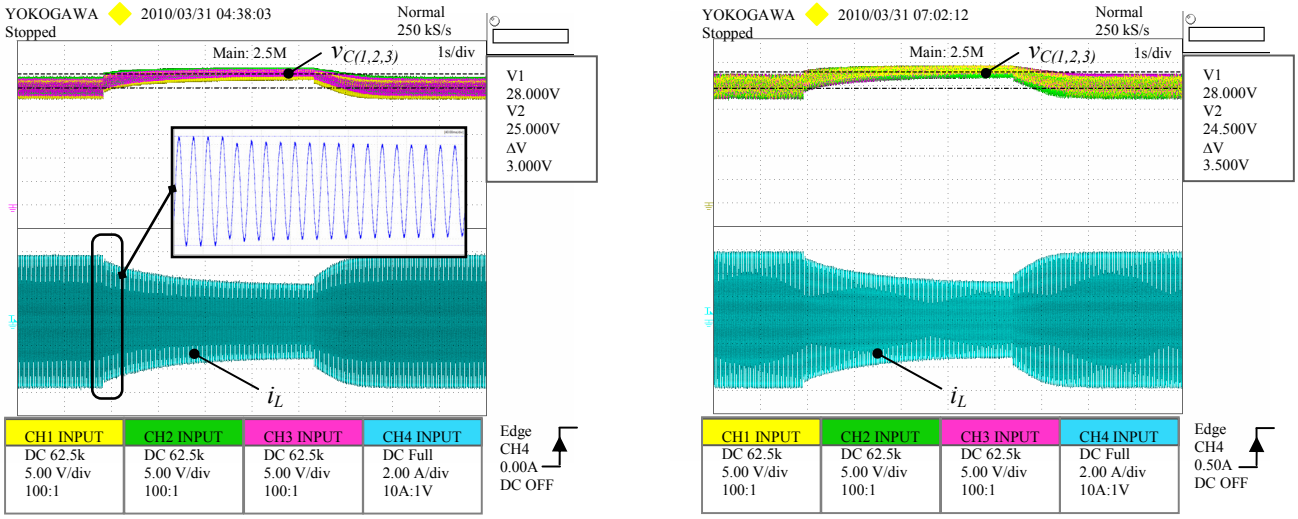

Figure 18. Capacitor voltage regulation. Inductor current (i_L) and capacitor voltages (v_{C1}, v_{C2} and v_{C3}) for both PS-PWM (left) and LS-PWM (right).

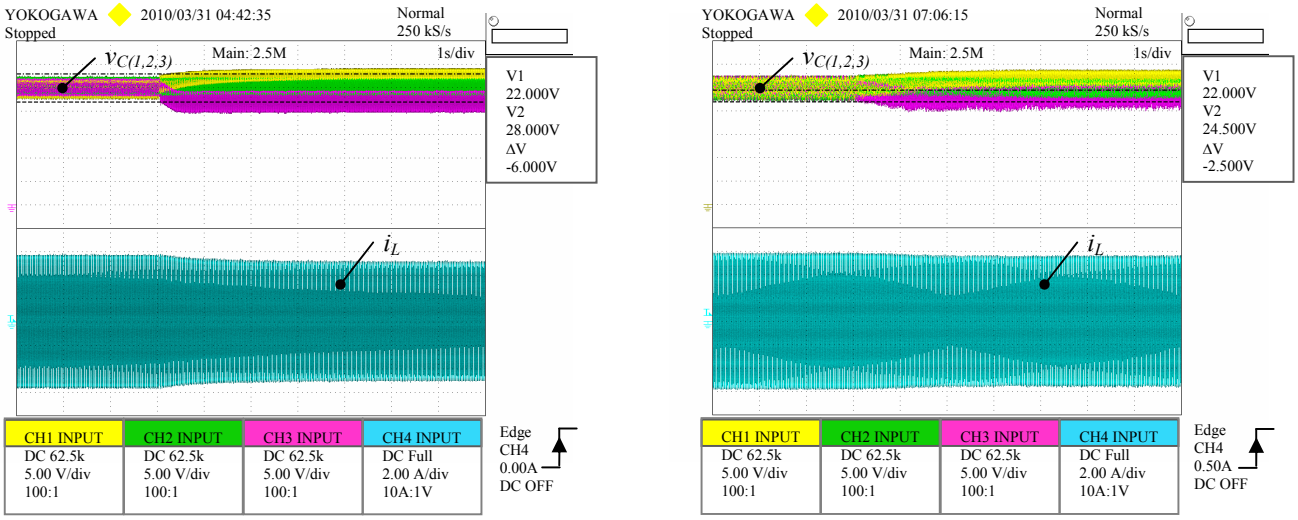

Figure 19. Capacitor voltage regulation. Inductor current (i_L) and capacitor voltages (v_{C1}, v_{C2} and v_{C3}) for both PS-PWM (left) and LS-PWM (right).